A&A 434, 397–404 (2005)
DOI: 10.1051/0004-6361:20042174

Astronomy & Astrophysics

Bowen excitation of N III lines in symbiotic stars

M. Eriksson[1,2], S. Johansson[2], G. M. Wahlgren[2], H. Veenhuizen[1], U. Munari[3], and A. Siviero[3]

[1] University College of Kalmar, 391 82 Kalmar, Sweden
[2] Atomic Astrophysics, Lund Observatory, Lund University, Box 43, 221 00 Lund, Sweden
[3] INAF, Osservatorio Astronomico di Padova, Sede di Asiago, 36012 Asiago (VI), Italy

Received 14 October 2004 / Accepted 3 December 2004

Abstract. We present a semi-empirical equation for prediction of the strengths of those N III lines that are generated by the Bowen mechanism and observed in spectra of symbiotic stars. The equation assumes that the Bowen mechanism is the only source populating the 3d state in N III, and comparisons with observations of the 3s–3p and 3p–3d transitions serve as a test of this assumption. In an ongoing study of symbiotic stars the equation has been applied to two symbiotic novae, RR Tel and AG Peg, by comparing the predicted N III line strengths to observed line intensities. It is clear that besides the Bowen mechanism there is another process, most likely radiative recombination, that contributes to the N III 3d population in AG Peg and is the main population process of this state in RR Tel. It is also clear that a second, not previously considered, N III channel, 2p $^2P_{1/2}$–3d $^2D_{3/2}$ at 374.198 Å, is pumped by O III in both RR Tel and AG Peg.

Key words. atomic processes – line: formation – binaries: symbiotic

1. Introduction

Optical O III and N III lines from highly excited levels are frequently observed as prominent features between 2800 and 4700 Å in spectra of gaseous nebulae. These lines have for a long time been understood as fluorescence lines (Bowen 1934, 1935), and they are usually referred to as "the Bowen excited lines". Although most investigations confirm the identification of the O III lines as He II pumped fluorescence lines (Saraph & Seaton 1980; Kastner & Bhatia 1990), a study of the N III lines in planetary nebulae (Kastner & Bhatia 1991) seems to exclude a similar interpretation for them. In this work the N III lines have been investigated in two symbiotic novae to determine the excitation mechanism behind them.

Under specific nebular conditions, photons from He II Lyα at 303.783 Å photo-excite O III from the ground term level 2p^2 $^3P_2$ to 2p3d $^3P_2$ at ∼40 eV through the λ303.800 channel (Fig. 1). Unno (1955) showed that considering broadening of He II Lyα by scattering, the 2p3d $^3P_1$ level can also be populated by pumping in the O III λ303.695 channel. Bowen excited lines are most frequently observed in emission in spectra of planetary nebulae (Aller et al. 1963), where the 2p3p ^{3}P–2p3d ^{3}P lines at ∼3400 Å were observed before the advent of satellite UV spectroscopy. With extended ultraviolet wavelength coverage it is now possible to detect all the 3s–3p and 3p–3d multiplets of O III, confirming that the Bowen mechanism is operating in many planetary nebulae. In Bowen's (1934, 1935) early work on O III a second step was proposed. When the pumped O^{2+} ions decay back from 2p3d to the ground term via 2p3p and 2p3s they emit the 2p^2 ^{3}P–2p3s ^{3}P extreme ultraviolet multiplet in the final step (see Fig. 1). One of the multiplet lines, ($^3P_2$–$^3P_1$) at 374.432 Å, coincides in wavelength with a transition from the ground state to 3d in N III and can photo-excite both of the fine-structure levels through the 2p–3d channels $\lambda\lambda$374.434, 374.442. However, even though 3p–3d transitions of N III are often observed in planetary nebulae, their relative intensities are closer to what is expected from a thermal Boltzmann population of the 3d levels than from a selective photoexcitation by the second pumping scheme in the Bowen mechanism (Kastner & Bhatia 1991).

The O III Bowen excited lines have also been observed in symbiotic stars (Wallerstein et al. 1991), and the mechanism behind their formation is discussed in detail by Pereira et al. (1999). They show that the efficiency of the Bowen mechanism increases with electron density and fractional abundance of ionized helium. Even if the N III 3s–3p and 3p–3d lines are observed in some symbiotic systems, it is not clear whether their presence is caused by the second pumping scheme of the Bowen process or if any other process is responsible for the 3d population. In the present study of AG Peg and RR Tel, the measured *FWHM* of ∼45 km s^{-1} of the O III and N III lines is smaller than for lines associated with the white-dwarf wind, which typically have *FWHM* values of ∼750 km s^{-1}. Still, the O^{2+} and N^{2+} ions must be formed in a region that is subjected to the ionizing radiation from the white dwarf such as the extended atmosphere of the red giant facing the white dwarf or parts of the nebula that are visible from the white dwarf.

In this work we present a model that predicts relative line strengths of the N III 3s–3p and 3p–3d lines assuming that the 3d levels are exclusively populated by the Bowen mechanism.

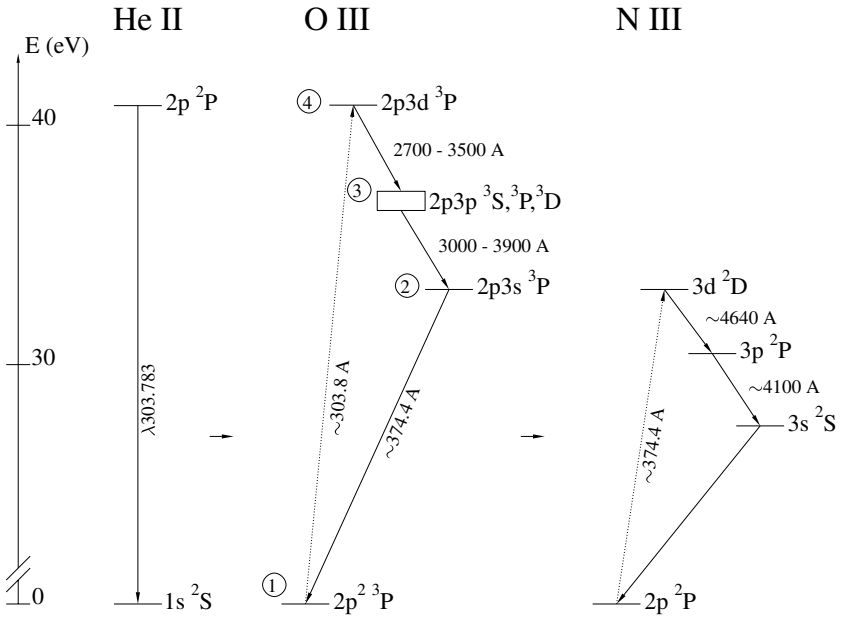

Fig. 1. Simplified picture of the Bowen mechanism.

Since the model is semi-empirical and requires observed data, spectra from 3000 Å to 4000 Å are used to measure the intensities of the 2p3s–2p3p lines. Also, data of good quality are needed to derive Gaussian line widths and relative shifts of the N III and O III lines. Not only the two known channels in N III pumped by O III are considered. All seven lines of the O III $2p^2\ ^3P$–$2p3s\ ^3P$ multiplet are treated as possible pumps of the three N III 2p–3d channels.

2. Data

To perform this work we needed spectra covering both the wavelength region of the O III Bowen excited lines (2800–3900 Å) and of the N III Bowen excited lines (4100–4700 Å). Two of the three O III Bowen multiplets studied fall in the wavelength region covered by the Long Wavelength Prime (LWP) camera of the International Ultraviolet Explorer (*IUE*) satellite. All line intensities of the two O III 2p3s–2p3p multiplets, ^3P–^3S and ^3P–^3P, were measured in the spectra LWP25995 (AG Peg) and LWP25954 (RR Tel). The line intensities of the third multiplet, ^3P–^3D, are taken from the literature (McKenna et al. 1997). The N III and O III lines used to derive widths and relative velocity shifts are all in the wavelength region of the Short Wavelength Prime (SWP) camera of the *IUE* satellite, and they were measured in the *IUE* spectra SWP54749 (AG Peg) and SWP29535 (RR Tel).

High resolution, absolutely flux calibrated spectra of AG Peg were recorded on 2002 Aug. 13 and 14, with the Echelle+CCD spectrograph of the 1.82 m telescope operated in Asiago, Italy by the INAF Astronomical Observatory of Padova. A total of 15 individual spectra have been combined into two spectra (one per night) of 7110 s total exposure time. They are electronically available[1], where further information is provided. The resolving power of the spectra is 20 000 and the brightness of AG Peg derived from the calibrated spectra is $v = 10.48$, $b = 9.54$, $y = 8.73$ in the Strömgren system. Intercomparison of the standard star and the AG Peg spectra for the two consecutive nights shows that the broad-band flux scale should be accurate to better than 0.025 mag (~2%) over most of the recorded spectral range. Figure 2 presents an extraction of the AG Peg spectrum around some N III lines.

The wavelengths of the O III $2p^2\ ^3P$–$2p3s\ ^3P$ transitions are taken from Pettersson (1982), who studied the O III spectrum in the 500–8500 Å region. He also derived Ritz wavelengths for lines in the 228–500 Å region from optimized energy levels. For this optimization he used his own measurements for the excited system (Pettersson 1982), astrophysical measurements of forbidden transitions between the fine structure levels of the ground term (Moorwood et al. 1980) and direct measurements of the lines connecting the excited system with the ground term (Edlén 1934). These Ritz wavelengths are estimated to be correct to about 0.005 Å at 250 Å and to 0.02 Å at 500 Å (Pettersson 1982), the difference reflecting the $(\Delta\lambda)^2$ dependence on the fixed uncertainty in the energy level values. Interpolation gives a wavelength uncertainty of 0.0012 Å for the O III $2p^2$–2p3s transitions at 374 Å. The wavelengths for the pumped N III $2p\ ^2P$–$3d\ ^2D$ transitions are taken from Michels (1974), which are claimed to be accurate to 0.005 Å.

We want to draw the reader's attention to the unreasonable uncertainty of 0.00009 Å given for the O III lines in the Internet database located at `http://www.pa.uky.edu/~peter/atomic/`. This value is more than 100 times better than the realistic estimate given by Pettersson (1982), and it demonstrates the danger of giving a general recipe for calculation of uncertainties. The wavelength uncertainty of a measured ultraviolet line can be considerably improved in complex, level-rich spectra by using the Ritz wavelength, but only slightly improved for ground term transitions in p-shell spectra.

[1] At `http://ulisse.pd.astro.it/AG_Peg/`

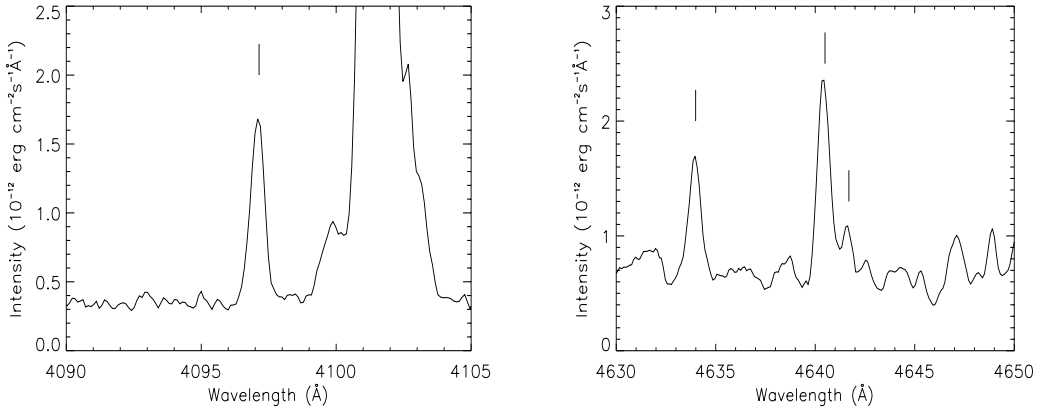

Fig. 2. Spectrum of AG Peg. *Left*: the line at 4097 Å is N III 3s $^2S_{1/2}$–3p $^2P_{3/2}$ while the 3s $^2S_{1/2}$–3p $^2P_{1/2}$ line is masked by Hδ at 4101 Å. *Right*: all three N III 3p–3d lines (4634–4642 Å) are observed.

3. Semi-empirical calculation of the N III Bowen excited lines

The procedure to obtain predictions of the relative strengths of the N III 3s–3p and 3p–3d lines involves observational data on the O III 2p3s–2p3p line intensities, the O III and N III line widths and, if any, the relative velocity shift between the O III and N III lines (see Fig. 1). The main steps of the procedure are:

1. estimate the relative line strengths of the O III 2p^2–2p3s transitions from the observed 2p3s–2p3p line intensities;
2. estimate the relative population rate of the N III 3d levels using observed widths and shifts of the O III and N III lines combined with the estimated O III 2p^2–2p3s line strengths;
3. prediction of the relative strengths of the N III Bowen excited lines.

3.1. Estimated relative strength of the O III 2p^2 ^{3}P–2p3s ^{3}P transitions

We consider the closed radiative cycle of O III in Fig. 1 under steady-state conditions and can express the population rates, dN_k/dt (k = 1–4), for the four states. In the actual case, as shown in Fig. 2, the states represent several fine structure levels, which are all taken into account in the full treatment. We denote the population of the states by N_k, the transition probabilities by A_{ik}, and the photoexcitation rate provided by He II Lyα is set to $W_{14}^{\rm exc}$. We introduce the concepts *feeding rate*, R_k^+, and *decay rate*, R_k^-, for state k through

$$\begin{aligned} R_k^+ &= N_{k+1} \cdot g_{k+1} \cdot A_{k+1,k} \;\; (k = 1{-}3) \\ R_4^+ &= W_{14}^{\rm exc} \\ R_k^- &= N_k \cdot g_k \cdot A_{k,k-1} \;\; (k = 2{-}4) \end{aligned} \tag{1}$$

where g_k are statistical weights. We assume that all transitions are optically thin and that collisional processes are negligible. Under steady-state conditions $dN_k/dt = 0$, and

$$dN_2/dt = 0 \;\rightarrow\; R_2^+ = R_2^- \;\rightarrow\; N_3 \cdot g_3 \cdot A_{32} = N_2 \cdot g_2 \cdot A_{21}. \tag{2}$$

The pumped 2p3d ^{3}P term has a primary decay to the 2p3p terms ^{3}S, ^{3}P and ^{3}D, which then decay to the 2p3s ^{3}P term as illustrated in Fig. 3. We estimate the relative strengths of the various transitions from 3s (state 2) to 2p (state 1) by applying Eq. (2) to the individual ^3P_i levels of 3s. The feeding rates, $R_2^+(i)$, are obtained from the observed intensities, $I_i(L_J)$ i = 0, 1, 2, of the 3p^{3}L$_J$–3s^{3}P$_i$ transitions

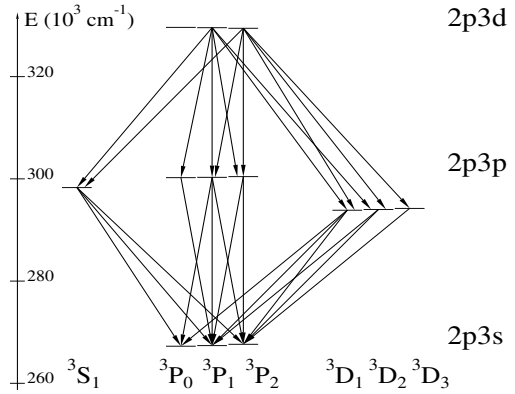

Fig. 3. Figure illustrating the Bowen primary and secondary decay in O III.

$$R_2^+(i) = R_i(\mathrm{S}_1) + \sum_{J=0}^{2} R_i(\mathrm{P}_J) + \sum_{J=1}^{3} R_i(\mathrm{D}_J), \tag{3}$$

where

$$R_i(\mathrm{L}_J) \propto I_i(\mathrm{L}_J) \cdot \lambda_i(\mathrm{L}_J). \tag{4}$$

We have not explicitly excluded those iJ-combinations in Eq. (3) that correspond to forbidden transitions. However, they do not contribute to $R_2^+(i)$ as their A-values are many orders of magnitude lower than for the allowed transitions.

The relative strength of the 2p3s ^3P_i–2p^2 ^3P_j transitions, I_{ij}, can now be estimated from the decay rates, $R_2^-(i) = R_2^+(i)$, by distributing the decay of the 3s levels (i) to the 2p levels (j) using the branching fractions, BF_{ij}, and compensating for the wavelength dependence (see Eq. (4)). We normalize to the intensity of the 2p3s $^3P_2$–2p^2 $^3P_1$ transition by setting I_{21} = 1. We obtain

$$I_{ij} = \frac{\lambda_{ij} \cdot BF_{ij} \cdot R(i)}{\lambda_{21} \cdot BF_{21} \cdot R^+(2)} \cdot I_{21}, \tag{5}$$

Table 1. Transitions probabilities and branching fractions of the O III $2p^2\ ^3P_i$–$2p3s\ ^3P_j$ transitions.

Transition	λ (Å)	A^a (s^{-1})	BF
$^3P_2$–$^3P_1$	374.432	1.754×10^9	0.417
$^3P_1$–$^3P_0$	374.328	4.204×10^9	1.000
$^3P_1$–$^3P_1$	374.162	1.050×10^9	0.250
$^3P_2$–$^3P_2$	374.073	3.156×10^9	0.750
$^3P_0$–$^3P_1$	374.004	1.401×10^9	0.333
$^3P_1$–$^3P_2$	373.803	1.052×10^9	0.250

[a] The transition probabilities are taken from Aggrawal et al. (1997).

where

$$BF_{ij} = \frac{A_{ij}}{\sum_j A_{ij}}. \quad (6)$$

The branching fractions are based on A-values calculated by the CIV3 program (Aggarwal et al. 1997), and they are presented in Table 1.

3.2. Predicted relative strengths of the N III 3s–3p and 3p–3d transition

The N^{2+} ions have three channels from the ground configuration $2s^22p$ to $2s^23d$, $^2P_{1/2}$–$^2D_{3/2}$ at 374.198 Å, $^2P_{3/2}$–$^2D_{3/2}$ at 374.442 Å and $^2P_{3/2}$–$^2D_{5/2}$ at 374.434 Å. If F^{ij}_{mn} represent the number of photons per second emitted by the O III $2p^2\ ^3P_i$–$2p3s\ ^3P_j$ that pumps N III through the channel $2p\ ^2P_m$–$3d\ ^2D_n$, then the total feeding rate $R^+_{D_n}$ of the N III level $3d\ ^2D_n$ (n = 3/2 or 5/2) through photoexcitation can be written as

$$P(^2D_n) = \sum_{m=1/2}^{3/2} \sum_{i=0}^{2} \sum_{j=i-1}^{i+1} F^{ij}_{mn}. \quad (7)$$

The pumping rate F^{ij}_{mn} can be expressed in terms of the opacity, $\kappa_{mn}(\lambda)$, in the N III $2p\ ^2P_m$–$3d\ ^2D_n$ channel and the spectral and spatial distribution of the O III $2p^2\ ^3P_i$–$2p3s\ ^3P_j$ line intensity ($I^{ij}(\lambda, r)$) as

$$\mathrm{d}(\mathrm{d}F^{ij}_{mn}) = (\kappa_{mn}(\lambda) \cdot I^{ij}(\lambda, r)\mathrm{d}\lambda)\mathrm{d}r. \quad (8)$$

Assuming that the intensities I^{ij} are constant throughout the N III region, $r = L$, and Eq. (8) is simplified to

$$\mathrm{d}F^{ij}_{mn} = L \cdot \kappa_{mn}(\lambda) \cdot I^{ij}(\lambda)\mathrm{d}\lambda. \quad (9)$$

The constant L is then only a geometrical characteristic of the O III/N III region that will be the same for all F^{ij}_{mn}. Assuming Gaussian profiles, the two functions, $\kappa_{mn}(\lambda)$ and $I^{ij}(\lambda)$, can be expanded to $\kappa_{mn} \cdot \phi_{mn}(\lambda)$ and $I^{ij} \cdot \theta^{ij}(\lambda)$, respectively, and Eq. (9) can then be expressed as

$$\mathrm{d}F^{ij}_{mn} = L \cdot \kappa_{mn} \cdot \phi_{mn}(\lambda) \cdot I^{ij} \cdot \theta^{ij}(\lambda)\mathrm{d}\lambda \quad (10)$$

where

$$\begin{cases} \kappa_{mn} = \dfrac{\pi \cdot e^2 \cdot f_{mn} \cdot n_m}{m \cdot c \cdot w_{\mathrm{N}}} \\ \phi_{mn}(\lambda) = \exp\left(-\dfrac{(\lambda_{mn} \cdot (1 - \frac{v}{c}) - \lambda)^2}{w^2_{\mathrm{N}}}\right) \\ I^{ij} = k_1 \cdot I_{ij} \\ \theta^{ij}(\lambda) = \exp\left(-\dfrac{(\lambda_{ij} - \lambda)^2}{w^2_{\mathrm{O}}}\right). \end{cases} \quad (11)$$

In Eq. (11) w_{O} and w_{N} are the Gaussian widths of the O III and N III lines, respectively, and f_{mn} is the oscillator strength of the $2p\ ^2P_m$–$3d\ ^2D_n$ transition. I^{ij} is the peak intensity and I_{ij} is the estimated relative strength, as predicted by Eq. (5), of the O III $2p^2$–$2p3s\ ^3P_i$–^3P_j transitions. The velocity of the N^{2+} ions relative to the O^{2+} ions is given by $\frac{v}{c}$ and n_m is the population of the N III $2p\ ^2P_m$ level, which is proportional to the statistical weight, ($n_m = n_0 g_m$), given the small fine structure splitting of the $2p\ ^2P$ term. k_1 and n_0 are constants and will not affect the relative values of the different F^{ij}_{mn}. The population rates can now be expressed as

$$F^{ij}_{mn} = \frac{L \cdot \pi \cdot e^2 \cdot k_1 \cdot k_2 \cdot f_{mn} \cdot g_m \cdot I_{ij}}{m_{\mathrm{e}} \cdot c \cdot w_{\mathrm{N}}} \times \int_{-\infty}^{\infty} \exp\left(-\frac{(\lambda_{mn} \cdot (1 - \frac{v}{c}) - \lambda)^2}{w^2_{\mathrm{N}}}\right) \exp\left(-\frac{(\lambda_{ij} - \lambda)^2}{w^2_{\mathrm{O}}}\right) \mathrm{d}\lambda.$$

Taking all parameters that are independent of indices i, j, m and n as a constant, K, the final expression for F^{ij}_{mn} is

$$F^{ij}_{mn} = K \cdot f_{mn} \cdot g_m \cdot I_{ij} \cdot \exp\left(-\frac{(\lambda_{mn} - \lambda_{ij} - \frac{v \cdot \lambda_{mn}}{c})^2}{w^2_{\mathrm{O}} + w^2_{\mathrm{N}}}\right). \quad (12)$$

The uncertainty of the F^{ij}_{mn} induced by the 0.005 Å uncertainty (see Sect. 2) of the involved wavelengths is roughly 28%, assuming a line width of 20 km s^{-1} for the O III and N III lines. The oscillator strengths (0.3900, 0.0391 and 0.3513 for $f_{1/2,3/2}$, $f_{3/2,3/2}$ and $f_{3/2,5/2}$, respectively) adopted here are taken from the theoretical calculations by Bell et al. (1995), who quoted their accuracy to be a few percent. To avoid underestimation of errors we will use 10% as the accuracy for the oscillator strengths for the purpose of uncertainty of the F^{ij}_{mn}. The calculated relative strengths of the O III pumping lines ($2p^2$–$2p3s$) depend critically on precise measurement of the intensities of the lines due to secondary decay in the Bowen mechanism (2p3s–2p3p). To derive the F^{ij}_{mn} by Eq. (10) measurements of the widths of the O III and N III lines as well as the relative velocity shift between the two spectra are needed.

The feeding rates $R^+_{D_n}$ of the $3d\ ^2D_n$ levels that can be obtained from Eq. (12) are now used to derive the relative decay rates $R^-_{\mathrm{D}}(n)$ of the $3d\ ^2D_n$ levels among the $3p\ ^2P_t$–$3d\ ^2D_n$ channels,

$$R^-_{\mathrm{D}}(n, t) = R^+_{\mathrm{D}}(n) \cdot BF_{tn}, \quad (13)$$

and the corresponding line intensities $I(^2D_n$–$^2P_t)$, normalized so that $I(^2D_{5/2}$–$^2P_{3/2}) = 1$ are given by

$$I(^2P_t - {}^2D_n) = \frac{\lambda(^2D_{5/2} - {}^2P_{3/2})}{\lambda(^2D_n - {}^2P_t)} \cdot \frac{R^-_{\mathrm{D}}(n, t)}{R^-_{\mathrm{D}}(5/2, 3/2)} \quad (14)$$

Table 2. Branching fractions of the N III 3s–3p and 3p–3d transitions.

Transition	λ (Å)	A (s^{-1})	BF
2p $^2P_{3/2}$–3d $^2D_{5/2}$	374.434	1.114×10^{10}	0.9927
2p^3 $^4S_{3/2}$–3d $^2D_{5/2}$	1243.056	1.717×10^{1}	1.5×10^{-9}
2p^3 $^2D_{5/2}$–3d $^2D_{5/2}$	1558.375	4.830×10^{4}	4.3×10^{-6}
2p^3 $^2D_{3/2}$–3d $^2D_{5/2}$	1558.723	3.011×10^{3}	2.7×10^{-7}
2p^3 $^2P_{3/2}$–3d $^2D_{5/2}$	2713.975	1.301×10^{6}	1.2×10^{-4}
3p $^2P_{3/2}$–3d $^2D_{5/2}$	4640.644	8.029×10^{7}	0.0072
2p $^2P_{1/2}$–3d $^2D_{3/2}$	374.198	9.290×10^{9}	0.8272
2p $^2P_{3/2}$–3d $^2D_{3/2}$	374.442	1.859×10^{9}	0.1655
2p^3 $^4S_{3/2}$–3d $^2D_{3/2}$	1243.143	3.156×10^{0}	2.8×10^{-10}
2p^3 $^2D_{5/2}$–3d $^2D_{3/2}$	1558.551	4.924×10^{3}	4.4×10^{-7}
2p^3 $^2D_{3/2}$–3d $^2D_{3/2}$	1558.859	4.747×10^{4}	4.2×10^{-6}
2p^3 $^2P_{1/2}$–3d $^2D_{3/2}$	2714.071	1.083×10^{6}	9.6×10^{-5}
2p^3 $^2P_{3/2}$–3d $^2D_{3/2}$	2714.388	2.159×10^{5}	1.9×10^{-5}
3p $^2P_{1/2}$–3d $^2D_{3/2}$	4634.126	6.718×10^{7}	0.0060
3p $^2P_{3/2}$–3d $^2D_{3/2}$	4641.851	1.337×10^{7}	0.0012
2s2p^2 $^4P_{1/2}$–3p $^2P_{3/2}$	530.464	3.018×10^{2}	1.3×10^{-6}
2s2p^2 $^4P_{3/2}$–3p $^2P_{3/2}$	530.632	2.118×10^{1}	9.0×10^{-8}
2s2p^2 $^4P_{5/2}$–3p $^2P_{3/2}$	530.861	7.533×10^{2}	3.2×10^{-6}
2s2p^2 $^2D_{5/2}$–3p $^2P_{3/2}$	691.193	9.606×10^{7}	0.4098
2s2p^2 $^2D_{3/2}$–3p $^2P_{3/2}$	691.225	1.064×10^{7}	0.0454
2s2p^2 $^2S_{1/2}$–3p $^2P_{3/2}$	871.862	3.733×10^{7}	0.1592
2s2p^2 $^2P_{1/2}$–3p $^2P_{3/2}$	1001.747	4.847×10^{5}	0.0021
2s2p^2 $^2P_{3/2}$–3p $^2P_{3/2}$	1002.853	2.215×10^{6}	0.0094
3s $^2S_{1/2}$–3p $^2P_{3/2}$	4097.355	8.769×10^{7}	0.3741
2s2p^2 $^4P_{1/2}$–3p $^2P_{1/2}$	530.565	2.599×10^{2}	1.1×10^{-6}
2s2p^2 $^4P_{3/2}$–3p $^2P_{1/2}$	530.733	7.959×10^{1}	3.4×10^{-8}
2s2p^2 $^2D_{3/2}$–3p $^2P_{1/2}$	691.397	1.065×10^{8}	0.4553
2s2p^2 $^2S_{1/2}$–3p $^2P_{1/2}$	872.135	3.749×10^{7}	0.1603
2s2p^2 $^2P_{1/2}$–3p $^2P_{1/2}$	1002.107	1.690×10^{6}	0.0072
2s2p^2 $^2P_{3/2}$–3p $^2P_{1/2}$	1003.214	9.164×10^{5}	0.0039
3s $^2S_{1/2}$–3p $^2P_{1/2}$	4103.393	8.730×10^{7}	0.3732

where $\lambda(^2D_n–^2P_t)$ is the wavelength of the 3d ^2D_n–3p ^2P_t transition. Then, the relative feeding rates of the 3p ^2P_t levels $R_P^+(t)$ are obtained by

$$R_P^+(1/2) = R_D^-(3/2, 1/2), \quad (15)$$

$$R_P^+(3/2) = R_D^-(3/2, 3/2) + R_D^-(5/2, 3/2). \quad (16)$$

Finally, the decay rates $R_P^-(t)$ and the strengths $I(^2P_t–^2S_{1/2})$ of the 3p ^2P_t–3s $^2S_{1/2}$ transitions can be estimated by,

$$R_P^-(t) = R_P^+(t) \cdot BF_{1/2,t}, \quad (17)$$

$$I(^2S_{1/2} -^2 D_n) = \frac{\lambda(^2D_{5/2} -^2 P_{3/2})}{\lambda(^2P_t -^2 S_{1/2})} \cdot \frac{R_P^-(t)}{R_D^-(5/2, 3/2)}, \quad (18)$$

where $\lambda(^2P_t–^2S_{1/2})$ is the wavelength of the 3s $^2S_{1/2}$–3p ^2P_t transition. All branching fractions, BF_{tn} and $BF_{1/2,t}$ are calculated by means of the Einstein coefficients provided by Bell et al. (1995) and are listed in Table 2. Figure 4 illustrates the cascades from the pumped 3d levels in N III.

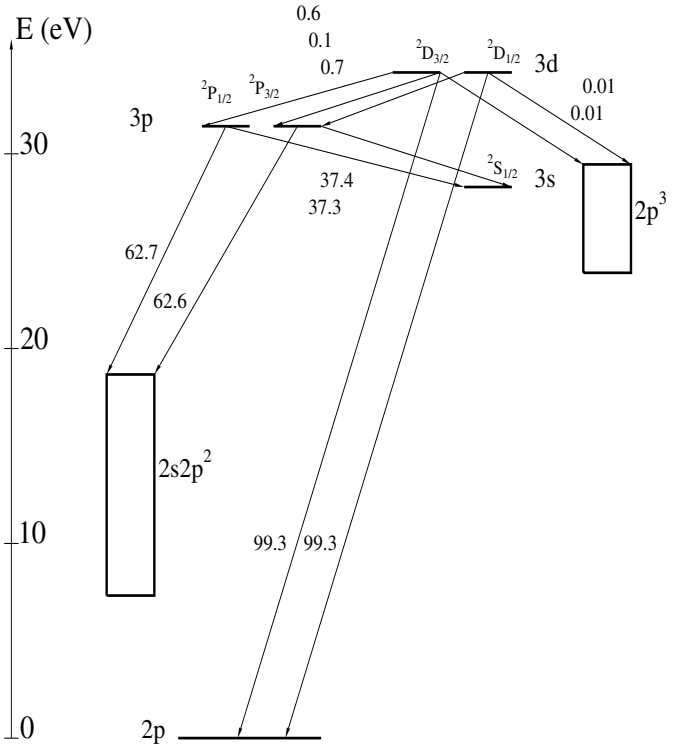

Fig. 4. The cascades from N III 3d levels. The percentage of the N^{+2} ions in the given levels that decay through the different channels is given in the figure.

4. N III Bowen line intensities compared to observations

4.1. AG Peg

In order to use Eq. (12), the relative strengths (I_{ij}) of the O III 2p^2 ^3P_i–2p3s ^3P_j transitions have to be estimated from the integrated intensities of the observed 2p3s–2p3p triplet lines. The second decay in the O III Bowen mechanism, 2p3s–2p3p, can form three multiplets, of which two are observed in AG Peg, ^{3}P–^{3}S (3300–3342 Å) and ^{3}P–^{3}P (3024–3061 Å). The third multiplet, ^{3}P–^{3}D (3755–3812 Å), is absent in the spectra and, to our knowledge, has not been observed in AG Peg. The population of the 2p3p ^{3}D levels is verified by the strong 2p3p ^{3}D–2p3d ^{3}D lines observed in the *IUE* spectra, and the 2p3p ^{3}D levels have no other allowed transitions than to the 2p3s ^{3}P levels. Therefore, it is strange that the 2p3s ^{3}P–2p3p ^{3}D multiplet is not observed. However, the absence of this multiplet indicates that its flux has to be at least one order of magnitude weaker than the other O III Bowen multiplets in AG Peg. In Table 3 all observed O III 2p3s–2p3p triplet transitions are listed. The relative intensity estimates, calculated from Eq. (5) of the 2p^2 ^3P_i–2p3s ^3P_j transitions are listed in Table 4. Since the N III and O III Bowen excited lines are observed in different spectra the N III] 2s^{2}2p ^{2}P–2s2p^2 ^{4}P and O III] 2s^{2}2p^2 ^{3}P–2s2p^3 ^{5}S transitions, located in the *IUE* (SWP) range, were selected as a measure of the relative velocity shift between the O^{2+} and N^{2+} ions. The Gaussian widths used for N III and O III spectra of AG Peg are 20.45 (±1.55) and 19.75 (±0.40) km s^{-1}, respectively, and the

Table 3. The relative intensity, I, and population rate, $R_i(L_j)$, of the O III 2p3s–2p3p triplet transitions observed in AG Peg.

Transition	λ (Å)	I (AG Peg)	$R_i(L_j)$ (AG Peg)	I (RR Tel)	$R_i(L_j)$ (RR Tel)
$^3P_2$–$^3D_1$	3810.99	0	0	0.49	0.19
$^3P_2$–$^3D_2$	3791.28	0	0	0.14	0.05
$^3P_1$–$^3D_1$	3774.03	0	0	0.09	0.03
$^3P_2$–$^3D_3$	3759.88	0	0	1.53[b]	0.58
$^3P_0$–$^3D_1$	3757.23	0	0	0.30	0.11
$^3P_1$–$^3D_2$	3754.70	0	0	0.29	0.11
$^3P_2$–$^3S_1$	3341.73	4.05	1.35	1.70	0.57
$^3P_1$–$^3S_1$	3313.28	1.68[a]	0.56	0.77[a]	0.26
$^3P_0$–$^3S_1$	3300.34	0.67	0.22	0.21	0.07
$^3P_2$–$^3P_1$	3060.17	0.93	0.28	0.40	0.12
$^3P_2$–$^3P_2$	3047.99	4.84	1.48	3.55	1.08
$^3P_1$–$^3P_0$	3042.95	0.19	0.06	0.08	0.02
$^3P_1$–$^3P_1$	3036.30	0.83	0.25	0.26	0.08
$^3P_0$–$^3P_1$	3025.42	0.85	0.26	0.36	0.11
$^3P_1$–$^3P_2$	3024.31	1.68	0.51	1.47	0.44

a) The λ3313 line is not observed since it falls between two orders in the IUE spectra. The strength is calculated by means of the measured intensity of the $\lambda\lambda$3341,3300 lines originating from the same upper level, and the branching fractions of the three ^{3}P–^{3}S transitions.
b) The line at 3759.87 Å in the AG Peg spectrum is dominated by [Fe VII]. The identification of this line in RR Tel (McKenna et al. 1997) as being mainly due to O III in RR Tel is not reasonable because of its large width and anomalous intensity. We conclude that this line is mainly due to [Fe VII] with some contribution from O III, and we have calculated an estimated intensity for this line (see text).

Table 4. Estimations of the relative intensity, I_{ij}, of the O III 2p^2 ^{3}P$_i$–2p3s ^{3}P$_j$ transitions.

Transition	λ (Å)	I_{ij} (AG Peg)	I_{ij} (RR Tel)
$^3P_2$–$^3P_1$	374.432	1.000	1.000
$^3P_1$–$^3P_0$	374.328	0.838	0.747
$^3P_1$–$^3P_1$	374.162	0.603	0.603
$^3P_2$–$^3P_2$	374.073	4.044	4.976
$^3P_0$–$^3P_1$	374.004	0.815	0.815
$^3P_1$–$^3P_2$	373.803	1.430	1.688

velocity shift used for the O III spectrum relative to the N III spectrum is -1.14 ($\pm$1.60) km s^{-1} (Table 5). The relative pumping rates (F^{ij}_{mn}) obtained from Eq. (12) are given in Table 6. The relative population rates of the two N III 3d ^{2}D$_n$ levels can then be derived from Eq. (13) with the result $R^+_{\rm D}(3/2)/R^+_{\rm D}(5/2)$ = 0.21. Table 8 lists the predicted Bowen intensities of the N III 3p–3d and 3s–3p lines by using Eqs. (13)–(18) and compares them to observed values. The last column lists the intensities of the same N III lines assuming that the population of the 3d ^{2}D levels is proportional to their statistical weights and that the 3p ^{2}P levels are populated by decay from those levels. Taking into consideration all uncertainties of the parameters involved in Eq. (12) leads to a total uncertainty of 37% for the relative pumping rates, which yields an uncertainty of 40% for the predicted N III 3p–3d and 3s–3p line intensities.

4.2. RR Tel

As for AG Peg the O III 2p3s–2p3p multiplets ^{3}P–^{3}S and ^{3}P–^{3}P are present in the *IUE* spectra of RR Tel. Also the third multiplet, ^{3}P–^{3}D, which was not observed in AG Peg, has been observed (McKenna et al. 1997). The relative intensities of all components in the 2p3s–2p3p multiplets measured in this work (Table 3) are used to derive estimates of the relative strengths of the 2p^2 ^{3}P–2p3s ^{3}P transitions (Table 4).

The λ3759 line in AG Peg has been identified as a [Fe VII] line (Kenyon et al. 2001). This is the same line that McKenna et al. (1997) identified as O III 2p3s ^{3}P$_2$–2p3p ^{3}D$_3$ in RR Tel. Since this line in the RR Tel spectrum is around two orders of magnitude stronger than the other O III Bowen excited lines and has a greater width we conclude that this line is predominantly due to [Fe VII] also in RR Tel. The strength of the O III 2p3s ^{3}P$_2$–2p3p ^{3}D$_3$ line has therefore been estimated as follows:

$$I_{\rm sp}(^3P_2{-}^3D_3) = \frac{I_{\rm pd}(^3D_3{-}^3P_2)\cdot I_{\rm sp}(^3P_1{-}^3D_2)}{BF_{\rm sp}(^3P_1{-}^3D_2)\cdot (I_{\rm pd}(^3D_2{-}^3P_2)+I_{\rm pd}(^3D_2{-}^3P_1))},$$

where the sp and pd indices refer to 2p3s–2p3p and 2p3p–2p3d transitions, respectively. The 2p3p–2p3d intensities involved have been measured in the *IUE* spectra, whereas the 2p3s–2p3p intensities are taken from McKenna et al. (1997).

The widths of the O III and N III lines used are 23.04 ($\pm$0.85) and 21.70 ($\pm$0.85) km s^{-1}, respectively, and they have been obtained from *IUE* spectrum SWP54749. The velocity shift between the O III and N III lines is 4.0 ($\pm$1.20) km s^{-1} (Table 5), obtained from the same spectrum. Using these values we get the pumping rates listed in Table 7, which leads to the relative population rates $R^+_{\rm D}(3/2)/R^+_{\rm D}(5/2)$ = 0.29 for RR Tel. The predicted values of the relative intensities of the N III 3p–3d and 3s–3p transitions are listed in Table 8, where they are compared to the stellar extinction corrected

Table 5. Velocity shift between N^{2+} and O^{2+} ions.

Spectra	λ_{obs} (Å)	λ_{id} (Å)	Width (km s^{-1})	Shift (km s^{-1})
AG Peg				
N III]	1753.828	1753.995	17.96	−28.56
N III]	1749.517	1749.674	20.58	−26.92
N III]	1748.486	1748.646	22.82	−27.45
O III]	1665.993	1666.150	19.63	−28.29
O III]	1660.647	1660.809	19.87	−29.27
RR Tel				
N III]	1753.581	1753.995	21.36	−70.81
N III]	1749.260	1749.674	21.78	−70.98
N III]	1748.223	1748.646	21.97	−72.57
O III]	1665.782	1666.150	23.31	−66.26
O III]	1660.429	1660.809	22.77	−68.64

The two O III] $2p^2\ ^3P$–$2s2p^3\ ^5S$ lines and the three strongest N III] $2p\ ^2P$–$2s2p^2\ ^4P$ lines are used to derive the velocity shift between O III and N III and the widths of the N III and O III lines. The observed lines are fitted with Gaussian profiles in the IUE (SWP) spectra No. 54749 for AG Peg and No. 29535 for RR Tel. The velocity shift, v and the widths w_N and w_O used in the equations are −1.14, 20.45 and 19.75 (AG Peg) and 4.0, 21.70 and 23.04 km s^{-1} (RR Tel).

Table 6. Pumping rates (F^{ij}_{mn}/K) as defined in Eq. (12) in AG Peg.

	$(m,\ n) = (1/2,\ 3/2)$	$(m,\ n) = (3/2,\ 3/2)$	$(m,\ n) = (3/2,\ 5/2)$
$(i,\ j) = (0,\ 1)$	1.70×10^{-14}	1.52×10^{-68}	2.37×10^{-65}
$(i,\ j) = (1,\ 0)$	7.22×10^{-7}	2.97×10^{-6}	7.50×10^{-5}
$(i,\ j) = (1,\ 1)$	0.1489	3.08×10^{-29}	6.44×10^{-27}
$(i,\ j) = (1,\ 2)$	1.85×10^{-55}	2.02×10^{-143}	4.10×10^{-139}
$(i,\ j) = (2,\ 1)$	9.81×10^{-20}	0.1395	1.3874
$(i,\ j) = (2,\ 2)$	4.27×10^{-6}	1.67×10^{-48}	1.09×10^{-45}

Table 7. Pumping rates (F^{ij}_{mn}/K) as defined in Eq. (12) in RR Tel.

	$(m,\ n) = (1/2,\ 3/2)$	$(m,\ n) = (3/2,\ 3/2)$	$(m,\ n) = (3/2,\ 5/2)$
$(i,\ j) = (0,\ 1)$	6.88×10^{-11}	6.29×10^{-54}	4.65×10^{-51}
$(i,\ j) = (1,\ 0)$	4.80×10^{-6}	5.94×10^{-5}	1.50×10^{-3}
$(i,\ j) = (1,\ 1)$	0.2537	7.52×10^{-23}	1.10×10^{-20}
$(i,\ j) = (1,\ 2)$	4.85×10^{-43}	1.92×10^{-113}	1.12×10^{-109}
$(i,\ j) = (2,\ 1)$	9.04×10^{-17}	0.1539	1.3971
$(i,\ j) = (2,\ 2)$	3.73×10^{-4}	8.45×10^{-38}	3.07×10^{-35}

values by McKenna et al. (1997). The uncertainties of the parameters in Eq. (12) lead to uncertainties for the predicted line strengths in RR Tel at 38%.

5. Conclusions

An interesting side result from the present work is that, besides the two previous known coincidences between O III λ374.432 and N III $\lambda\lambda$374.434, 374.442, a previously neglected coincidence between O III λ374.162 and N III λ374.198 is shown to be an active pumping channel, at least in RR Tel and AG Peg (Tables 6 and 7).

However, it is evident that there is a large difference both for AG Peg and RR Tel between the observed relative intensities and the predicted relative line strengths of the fluorescent N III $\lambda\lambda$4641, 4634 and 4097 lines assumed to be radiatively excited by the O III pumping in the second step of the Bowen mechanism. According to the data in Table 8, the deviation from pure radiative excitation for AG Peg is about the same, ≃60−70%, as the deviation assuming a pure statistical population of the fine structure levels. In RR Tel the observed intensities imply a deviation from pure Bowen fluorescence up to a factor of four, whereas the deviation from a statistical population is only ≈30%.

We conclude that the Bowen process is active in forming the N III lines in AG Peg but that other processes also are populating the 3d levels. The 3d $^2D_{3/2}$ level has a higher population relative to 3d $^2D_{5/2}$ than what is predicted assuming a pure Bowen process population, but lower than what is expected for thermal conditions. For RR Tel the N III 3d levels seem to be

Table 8. Predicted relative intensities of the N III 3s–3p and 3p–3d lines assuming Bowen excitation compared to observed values.

Transition	λ_{air} (Å)	I_t (AG Peg)	I_o (AG Peg)[a]	I_t (RR Tel)	I_o (RR Tel)[b]	Stat.
$3p\ ^2P_{3/2}$–$3d\ ^2D_{5/2}$	4640.644	1.000	1.000	1.000	1.000	1.000
$3p\ ^2P_{3/2}$–$3d\ ^2D_{3/2}$	4641.851	0.035	0.042	0.049	0.199	0.111
$3p\ ^2P_{1/2}$–$3d\ ^2D_{3/2}$	4634.126	0.174	0.433	0.245	0.460	0.558
$3s\ ^2S_{1/2}$–$3p\ ^2P_{3/2}$	4097.355	0.438	0.592	0.444	0.430	0.471
$3s\ ^2S_{1/2}$–$3p\ ^2P_{1/2}$	4103.393	0.074	bl	0.103	bl	0.235

[a] Measured in this work; [b] measured by McKenna et al. (1997). The subscript "t" refers to the predicted intensity assuming all N III lines are due to the Bowen mechanism, and the subscript "o" refers to the observed value. The last column lists the intensity of the lines assuming statistical equilibrium for the 3d ^{2}D levels. The N III λ4103.393 line is blended with the Hδ line.

predominantly populated by processes other than the Bowen mechanism.

It is clear that the main part of the large uncertainty in the predicted relative line strengths of the O III pumped N III lines in the Bowen mechanism can be ascribed to uncertainties in the wavelengths of the ground term transitions of O III and N III at 374 Å. The combined effect of wavelength uncertainties and relative velocity shifts on the overlap of the profiles of the pumping and the pumped lines introduces larger uncertainties than considered in previous work. Unfortunately, there is a little chance that the situation with the laboratory wavelength will improve in the near future. Also, we draw the readers' attention to the danger of using wavelength uncertainties claimed in some databases, as they are derived using incorrect principles.

The observation of the radiative decay from the 3d levels in N III is documented for many objects, and here we have reported strong lines in the spectra of RR Tel and AG Peg. The population of these levels by processes other than the Bowen mechanism is hard to explain. Since the excitation energy of the 3d levels is around 33.14 eV, collisional excitation can be ruled out. We are left with two possibilities, charge exchange with hydrogen or radiative recombination. Since charge exchange preferentially populates the 3s level (Butler & Dalgano 1980), radiative recombination seems to be the most probable additional process.

In AG Peg the N III λ4097.355 line is stronger than predicted but this is not the case for RR Tel. However, the state-specific recombination rate to the N III $2s^2 3p\ ^2P$ state is ~3.5 times higher than for the $2s^2 3d\ ^2D$ state (Nahar & Pradhan 1997). The N III λ4097.355 line should therefore be stronger than what is predicted, which seems to be the case for AG Peg but not for RR Tel. There are two problems with recombination as the explanation for deviations between the predicted and observed N III intensities. Since the observed intensity ratio $I(\lambda4641.851)/I(\lambda4640.644)$ in RR Tel is greater than predicted both by the Bowen mechanism and statistical weights, recombination cannot explain the observed ratio. Also, if we incorporate recombination to obtain predictions closer to the observed relative strengths for the three N III 3p–3d transitions, then the predicted strength of the N III 3s–3p transition at 4097.355 will be at least twice as strong as the N III λ4640.644 line for both RR Tel and AG Peg.

References

Aggarwal, K. M., Hibbert, A., & Keenan, F. P. 1997, ApJS, 108, 393
Aller, L. H., Bowen, I. S., & Wilsson, O. C. 1963, ApJ, 138, 1013
Bell, K. L., Hibbert, A., Stafford, R. P., & Brage, T. 1995, MNRAS, 272, 909
Bowen, I. S. 1934, PASP, 46, 146
Bowen, I. S. 1935, ApJ, 81, 1
Butler, S. E., & Dalgano, A. 1980, ApJ, 241, 838
Kastner, S. O., & Bhatia, A. K. 1990, ApJ, 362, 745
Kastner, S. O., & Bhatia, A. K. 1991, ApJ, 381, 59
Kenyon, S. J., Proga, D., & Keyes, C. D. 2001, AJ, 122, 349
McKenna, F. C., Keenan, F. P., Hambly, N. C., et al., 1997, ApJS, 109, 225
Michels, D. J. 1974, J. Opt. Soc. Am., 64, 1164
Nahar, N. N., & Pradhan, A. K. 1997, ApJS, 111, 339
Pereira, C. B., de Araújo, F. X., & Landaberry, S. J. C. 1999, MNRAS, 309, 1074
Pettersson, S. G. 1982, Phys. Scr., 26, 296
Saraph, H. E., & Seaton, M. J. 1980, MNRAS, 193, 617
Unno, W. 1955, PASJ, 7, 81
Wallerstein, G., Garnavich, P. M., Schacter, J., & Oke, J. B. 1991, PASP, 103, 185